

### Annual Review of Marine Science

# The Dissolution Rate of CaCO<sub>3</sub> in the Ocean

Jess F. Adkins, <sup>1</sup> John D. Naviaux, <sup>1</sup> Adam V. Subhas, <sup>2</sup> Sijia Dong, <sup>1</sup> and William M. Berelson <sup>3</sup>

<sup>1</sup>Linde Center for Global Environmental Science, Department of Geology and Planetary Sciences, California Institute of Technology, Pasadena, California 91125, USA; email: jess@gps.caltech.edu, dongsj@caltech.edu

<sup>2</sup>Department of Chemistry, Woods Hole Oceanographic Institution, Woods Hole, Massachusetts 02543, USA; email: asubhas@whoi.edu

<sup>3</sup>Department of Earth Sciences, University of Southern California, Los Angeles, California 90089, USA; email: berelson@usc.edu

Annu. Rev. Mar. Sci. 2021. 13:57-80

First published as a Review in Advance on September 18, 2020

The Annual Review of Marine Science is online at marine.annualreviews.org

https://doi.org/10.1146/annurev-marine-041720-092514

Copyright © 2021 by Annual Reviews. All rights reserved

### ANNUAL CONNECT

### www.annualreviews.org

- Download figures
- Navigate cited references
- · Keyword search
- · Explore related articles
- · Share via email or social media

### **Keywords**

lysocline, carbonate compensation, calcite, aragonite, alkalinity

#### Abstract

The dissolution of CaCO<sub>3</sub> minerals in the ocean is a fundamental part of the marine alkalinity and carbon cycles. While there have been decades of work aimed at deriving the relationship between dissolution rate and mineral saturation state (a so-called rate law), no real consensus has been reached. There are disagreements between laboratory- and field-based studies and differences in rates for inorganic and biogenic materials. Rates based on measurements on suspended particles do not always agree with rates inferred from measurements made near the sediment-water interface of the actual ocean. By contrast, the freshwater dissolution rate of calcite has been well described by bulk rate measurements from a number of different laboratories, fit by basic kinetic theory, and well studied by atomic force microscopy and vertical scanning interferometry to document the processes at the atomic scale. In this review, we try to better unify our understanding of carbonate dissolution in the ocean via a relatively new, highly sensitive method we have developed combined with a theoretical framework guided by the success of the freshwater studies. We show that empirical curve fits of seawater data as a function of saturation state do not agree, largely because the curvature is itself a function of the thermodynamics. Instead, we show that models that consider both surface energetic theory and the complicated speciation of seawater and calcite surfaces in seawater are able to explain most of the most recent data. This new framework can also explain features of the historical data that have not been previously explained. The existence of a kink in the relationship between rate and saturation state, reflecting a change in dissolution mechanism, may be playing an important role in accelerating CaCO<sub>3</sub> dissolution in key sedimentary environments.

### INTRODUCTION

Rivers carry the products of terrestrial weathering to the ocean, and processes at the ocean margins, mostly sedimentation, work to remove them. For the alkalinity budget of the ocean, this output flux is dominated by CaCO<sub>3</sub> sedimentation. Hydrothermal processes, both low and high temperature, play an important role (Elderfield & Schultz 1996), but the modern budget is dominated by riverine inputs and burial of carbonate shells produced in the upper ocean (Milliman 1993). The ecosystems that govern this production feel the input of alkalinity only indirectly, as the surface ocean is mostly supersaturated for both calcite and aragonite. As a consequence, the surface ocean overproduces alkalinity by a factor of two to four times relative to the amount coming in from rivers (Berelson et al. 2007, Milliman et al. 1999). Somewhere in the ocean, approximately 75% of all the mineral carbonate produced by corals, coccolithophores, foraminifera, and so on must dissolve. For many decades, this process has been assumed to happen primarily via carbonate compensation in the deep ocean (Broecker & Peng 1987). The solubilities of the two principal polymorphs made in the ocean, aragonite and calcite, are strongly pressure dependent, such that deep waters are more corrosive than shallow waters (Ben-Yaakov et al. 1974, Ingle 1975, Sayles 1985). Through a combination of relatively slow processes—the overturning circulation, bioturbation, and the CaCO<sub>3</sub> dissolution itself—the canonical timescale for this system to respond to changes is approximately 6,000 years (Archer et al. 1998, Ilyina & Zeebe 2012).

Challenges to this view of an alkalinity cycle controlled by the deep ocean have focused mainly on the production of highly soluble phases in the upper ocean. While pteropods are not common in sediments below the saturation horizon, they are produced ubiquitously in the upper ocean and could provide a water column source of CaCO3 dissolution (Bednaršek et al. 2014, Byrne et al. 1984, Fabry 1990). Fish must regulate their Ca ion channels around their gills and therefore produce an especially soluble form of carbonate in their excrement (Salter et al. 2019, 2017). An important observation that requires something about the cycle to be different from the canonical understanding comes from the distribution of tracer in the ocean itself. A value referred to as TA\* (Feely et al. 2002) subtracts off the effects of preformed alkalinity and the effects of organic matter remineralization from the measured, salinity-normalized total alkalinity in the ocean interior. These anomalies should track the input and removal of CaCO<sub>3</sub> along isopycnals. In their seminal paper, Feely et al. (2002) found large positive values of TA\* above the saturation horizon, especially in the North Pacific. Based on chlorofluorocarbon-constrained ventilation rates, the  $\sigma_{\theta}$  surface around 26.6 seems to have very high dissolution rates of CaCO<sub>3</sub>, implying that there is a robust shallow alkalinity cycle in the modern ocean even when the surrounding waters are supersaturated.

Even if a way to get around the thermodynamic constraint of supersaturation could be found—for instance, by shallow sedimentary dissolution at the ocean margins (Friis et al. 2006)—the kinetics of CaCO<sub>3</sub> dissolution are not well understood. A lack of either statistical or mechanism-based agreement in the community on the rate of CaCO<sub>3</sub> dissolution—either biogenic or inorganic, aragonite or calcite—limits our ability to understand the effects of increasing ocean acidification. We do not know how quickly CaCO<sub>3</sub> particles and sediments will be able to work to buffer the input of anthropogenic CO<sub>2</sub> as the pH of the upper and intermediate ocean drops (Feely et al. 2004).

Early efforts to describe the rate law in seawater (dissolution rate as a function of the degree of undersaturation) were essentially two-parameter curve fits rather than a mechanistic understanding of the elementary reactions that control the dissolution path (Keir 1980). However, some early work did postulate that PO<sub>4</sub> inhibition of the dissolving surface was the link between in situ observations and dissolution theory (Berner & Morse 1974, Morse & Berner 1972). The freshwater community has had more success defining how protons, carbonic acid, and water itself work to attack CaCO<sub>3</sub> surfaces in undersaturated waters (Arakaki & Mucci 1995), but there has not been a successful link of this work to the marine realm until very recently.

In this review, we hope to show how both the empirical approach to rate laws and an improved understanding of the mechanistic controls have drastically improved for seawater in the last few years. The ability to test surface dissolution rate theories with advanced nanoscale instrumentation, in combination with a new sensitive bulk dissolution rate method that works in seawater, can unify the ideas behind the mechanisms that control carbonate dissolution at the atomic scale. In addition, approaches that rely on in situ measurements of dissolution can now be aligned with laboratory studies that have more controlled environments but did not previously have the complications associated with real seawater. With this review, we hope to show a way forward for using carbonate dissolution rates in seawater as a stringent test for the emerging theoretical approaches that describe dissolution from first principles at the solid–solution interface. We also hope to bring the laboratory and in situ measurements back into agreement as they work to constrain the new theory.

### SOME HISTORY OF THE CACO3 DISSOLUTION RATE IN SEAWATER

The dissolution rate of  $CaCO_3$  in seawater was first and famously determined by Peterson (1966) during his hanging-spheres experiment conducted in the 1960s. He measured the mass loss of preweighed calcite samples during a four-month-long exposure to the North Pacific water column south of Hawaii, and his profile (**Figure 1**) shows initial dissolution at only a few hundred meters deep and then a large acceleration of the rate near 3,500 m. From this work, he correctly surmised that the bulk of the Pacific water column is undersaturated for calcite and related the large increase in rate at depth to the sedimentary lysocline. However, he did not have a good understanding of why the rates suddenly jumped at 3,500 m. He knew that the saturation state ( $\Omega$ ) was a smooth function of water depth and therefore guessed that it had something to do with masking and coating by other ions and molecules. Using the same mooring, Berger (1967) demonstrated that planktonic foraminifera shells have essentially the same behavior as the calcite spheres (**Figure 1**). By the end of this review, we hope to convince the reader that Peterson's data are still some of the best ever collected and reveal a tight relationship between in situ and laboratory-generated rates, as well as an important link between the behaviors of inorganic and biogenic carbonate dissolution rates.

During these early days of carbonate dissolution studies, the goal was to understand the sedimentary lysocline (where the percentage of  $CaCO_3$  in core tops drops dramatically) and its relation to the saturation horizon (where the water column saturation value for calcite changes from net precipitation to net dissolution). Kinetics of some sort must play a role because the drop from approximately 90%  $CaCO_3$  (approximately the value in raining particles) to 0%  $CaCO_3$  is not instantaneous with depth. Edmond (1974) hypothesized that the increase in rate seen by Peterson, as well as the sediment lysocline itself, was due to an increase in deep-water flow rates, perhaps pointing to the stagnation of waters immediately surrounding the spheres. After compiling the evidence for the pressure dependence of the calcite  $K_{sp}$ , Broecker & Takahashi (1978) believed that dissolution started at the saturation horizon and that a rapid increase in  $\Delta CO_3$  from approximately 0  $\mu$ mol/kg at 2.5 km to approximately 30  $\mu$ mol/kg at 5 km could explain

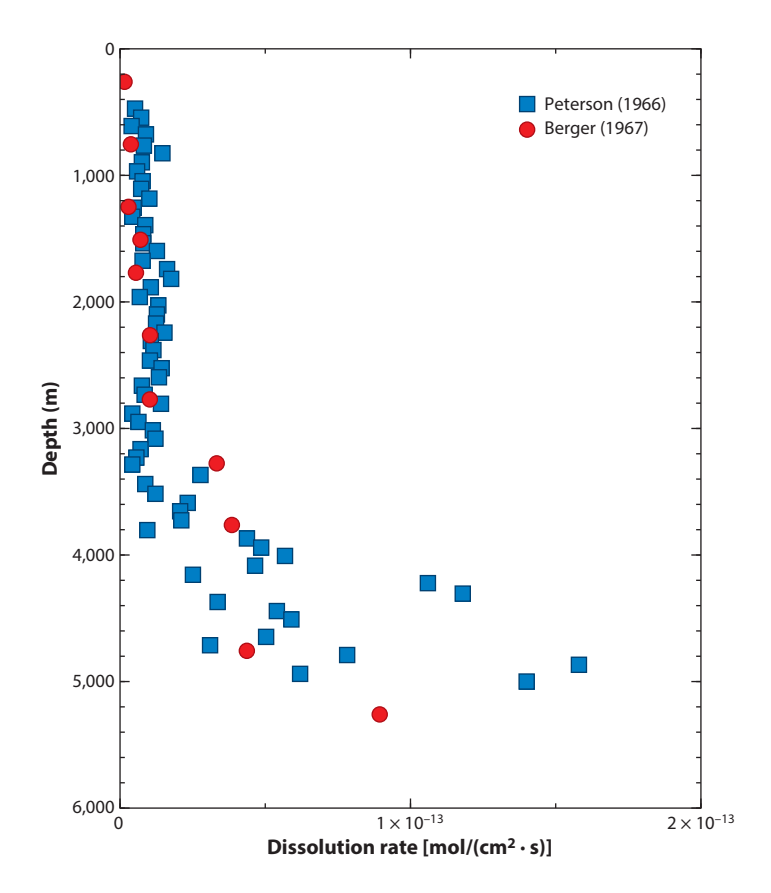


Figure 1

In situ results from Peterson (1966) (*squares*) and Berger (1967) (*circles*) for the dissolution rates of calcite spheres and planktonic foraminifera, respectively. The data were collected by weighing samples before and after they were hung on a moored wire in the North Pacific water column for four months. All data have been converted to flux units, which required using a specific surface area of 0.5 m<sup>2</sup>/g for Berger's foraminifera. This surface area is at the low end of BET measurements of other foraminifera samples (Honjo & Erez 1978, Keir 1980).

Peterson's data. In this sense, they believed that the lysocline was a thermodynamic feature of the ocean. This view was supported by the co-occurrence of the water column saturation horizon and the first shift from a higher to lower percentage of CaCO<sub>3</sub> (Berger et al. 1976, Biscaye et al. 1976, Kolla et al. 1976). Honjo & Erez (1978) built a new device with in situ pumping to rule out possible problems with stagnation around the CaCO<sub>3</sub> samples. They found a large increase in dissolution rate with depth, similar to Peterson's results, but also noticed that inorganic calcite dissolved faster than foraminifera, which in turn dissolved faster than coccoliths. These authors attributed the large offsets in specific (area-normalized) dissolution rate between their numbers and those of other workers to differences in the reactive surface areas of different samples. By the end of the review, we hope to convince the reader that, while many of these early observations and conclusions were pointing to real issues in the field, our modern understanding can unify the differences into a more coherent (though still incomplete) theory of carbonate dissolution rate.

Several authors have attempted to clarify the dissolution rate differences with laboratory experiments. John Morse and Bob Berner performed a landmark study on the controls determining

calcite dissolution rates as part of Morse's PhD thesis. Using synthetic seawater, not just solutions with high NaCl concentrations, Morse & Berner (1972) determined the dissolution rate via the pH-stat method, where pH control to within ±0.002 units led to a detection limit of 0.1%/h— a major innovation at the time. They found a critical pH change relative to equilibrium where the dissolution rate jumped sharply. This threshold value was theorized to be controlled by the adsorption of PO<sub>4</sub> ions on the calcite surface, which led to dissolution inhibition until a critical energetic barrier was crossed (Berner & Morse 1974). By relating this critical pH to Peterson's data, the authors concluded that the lysocline was fundamentally controlled by dissolution kinetics and not strictly the bottom-water CO<sub>3</sub> content. Keir (1980) continued the Yale tradition of laboratory-based rate measurements and found a nonlinear relationship between dissolution rate and calcite saturation state. Following Morse's (1978) initial curve fitting, Keir demonstrated that a wide range of inorganic and biogenic samples adhered to the rate law

$$rate = k(1 - \Omega)^n.$$

His data showed an offset in the rate constant for the different materials but a consistent value of n = 4.5.

Emerson & Bender (1981) proposed that respiration-driven dissolution above the saturation horizon, but in the top several centimeters of sediment, is an important control on the sedimentary lysocline. Their hypothesis breaks the direct link between bottom-water saturation state and the top of the lysocline, though we now understand that these two must remain coupled to some degree, if not at exactly the same depth (Sigman et al. 1998). This idea sparked a flurry of benthic technology development, with in situ microelectrodes (Archer et al. 1989, Cai et al. 1995, Hales et al. 1994), novel sampling devices to capture the chemical gradients at the sediment-water interface (Bender et al. 1987, Sayles et al. 1976), and benthic flux chambers (Berelson et al. 1987, Jahnke 1990) leading the way. Hales & Emerson (1997) argued for linear kinetics (n = 1) based on pore-water pH profile fits and a refit of Keir's laboratory-based data with a new  $K_{\rm sp}$  that was different from Mucci's (1983) classic work. Berelson et al. (1994) found CaCO3 dissolution rates in the equatorial Pacific that were consistent with Keir's original n = 4.5 result, setting up a long-standing discrepancy in the field. Recently, Boudreau and others have revived the idea that the benthic diffusive boundary layer is an important control on the flux of alkalinity back to bottom water from sedimentary carbonate dissolution (Boudreau 2013, Boudreau et al. 2020, Santschi et al. 1991, Sulpis et al. 2017). Boudreau et al. (2020) pointed out that, in the absence of respiration-driven dissolution, and also assuming linear kinetics, the existence of a boundary layer can make in situ measurements less sensitive to the reaction rate and order. Outside of the extremes of very thick boundary layers (termed sediment-side control) or very slow dissolution kinetics (termed waterside control), the flux of alkalinity back to the ocean from dissolution in sediments is a mixture of these two processes. Much of the literature to date has assumed either fast kinetics relative to diffusive fluxes at the sediment-water interface (Boudreau 2013, Boudreau et al. 2020) or thin enough boundary layers that only the chemistry in the sediments is important for setting alkalinity fluxes and, by extension, the shape of the lysocline (Archer 1991). Given the distribution of bottom currents (Sulpis et al. 2018) and the slow kinetics near equilibrium (Subhas et al. 2015), it is likely that the real ocean is affected by both the turbulent boundary-layer thickness (physics) and the reaction kinetics (chemistry) of the environment.

One outcome of the benthic studies and the focus on the sediment–water interface has been a general disagreement about the order and rate constant for carbonate dissolution. Both Keir and Morse found a high-order dependence (n > 1 in Equation 1) of calcite dissolution rates on  $\Omega$ . In a log–log plot, these high orders are the slope of the relation between rate and saturation state (**Figure 2***a*). Many curve fits have been proposed, sometimes using the same data to get very

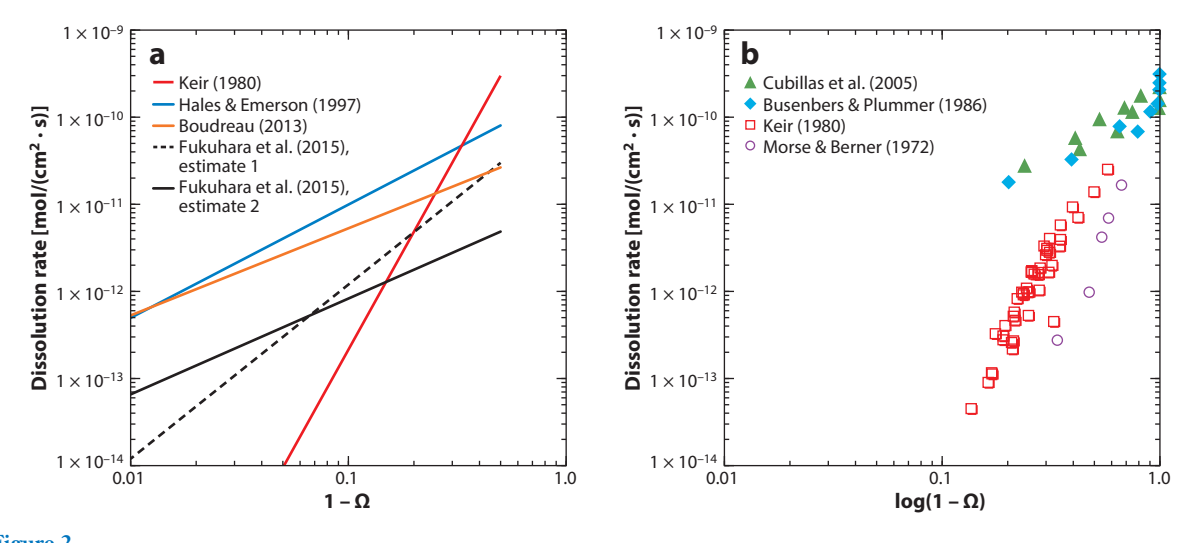


Figure 2

Some of the (a) curve fits and (b) data used to establish calcite dissolution rate laws in seawater and fresh water. The slopes and intercepts in panel a are the parameters n and k, respectively, in Equation 1. Within 20% of equilibrium  $(1 - \Omega = 0.2)$ , where most of the ocean's undersaturated water sits, there are almost no data, and curve fits disagree by well over  $100 \times$ . This is especially true for higher-order fits like those of Keir (1980) (red line) and close-to-linear fits like those of Hales & Emerson (1997) (blue line) or the assumed linear kinetics of Boudreau (2013) (orange line). Also shown are two estimates from Fukuhara et al.'s (2008) in situ deployments (solid black and dashed black lines). In panel b, open symbols are for seawater, showing data from Keir (1980) (squares) and Morse & Berner (1972) (circles); closed symbols are for fresh water, showing data from Cubillas et al. (2005) (triangles) and Busenberg & Plummer (1986) (diamonds).

different results (Boudreau 2013, Hales & Emerson 1997, Keir 1983). The literature has been left with a range of dissolution rates that span orders of magnitude near equilibrium, where most of the ocean's water column lies. However, most of the actual data that constrain these curve fits (**Figure 2***b*) have been collected relatively far from equilibrium, in both seawater and fresh water. There are two key messages from **Figure 2***b*. First, at the same saturation state, dissolution rates in fresh water are much faster than those in seawater. The complicated background electrolyte solution that is seawater has a clear effect on the dissolution rate over and above just the size of the thermodynamic driving force  $(1 - \Omega)$ . Second, the data constraining seawater curve fits (outside of Peterson's original study) do not cover the relevant range of real ocean  $\Omega$  values. It is not clear why Peterson's data have not been used in the bulk of the literature since his study, but one problem is probably the lack of good estimates of  $\Omega$  itself at the time of his work, along with a perception that stagnation around the particles influenced the rates. With the rising importance of ocean acidification (Feely et al. 2004) and the lack of understanding of why seawater and freshwater data are so far offset for the same saturation state, it was clear that this problem needed to be revisited.

## THERMODYNAMIC CONSTRAINTS ON DISSOLUTION RATE AND A NEW METHOD FOR MEASURING RATES IN SEAWATER NEAR AND FAR FROM EQUILIBRIUM

Given the need for precise measurements of CaCO<sub>3</sub> dissolution in seawater near equilibrium, Subhas et al. (2015) developed a novel <sup>13</sup>C-label method. We have used this approach to explore the basic thermodynamic controls on CaCO<sub>3</sub> dissolution rate, varying saturation state, temperature, and pressure. By placing purely labeled Ca<sup>13</sup>CO<sub>3</sub> into gas-impermeable bags with no head space,

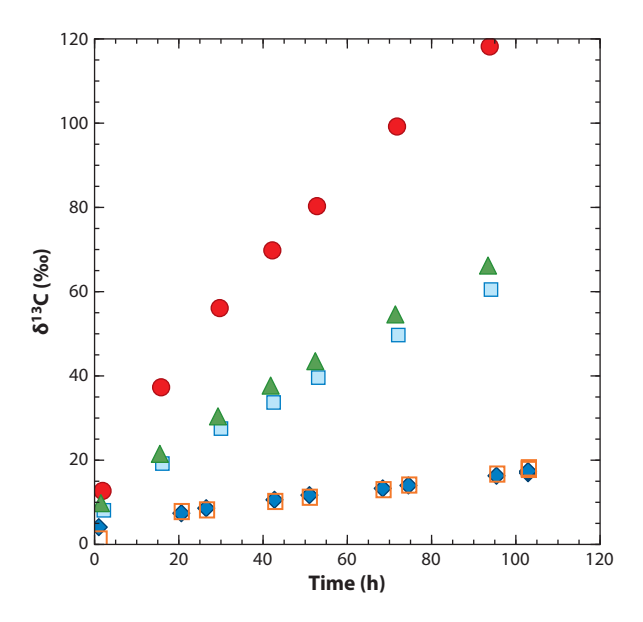
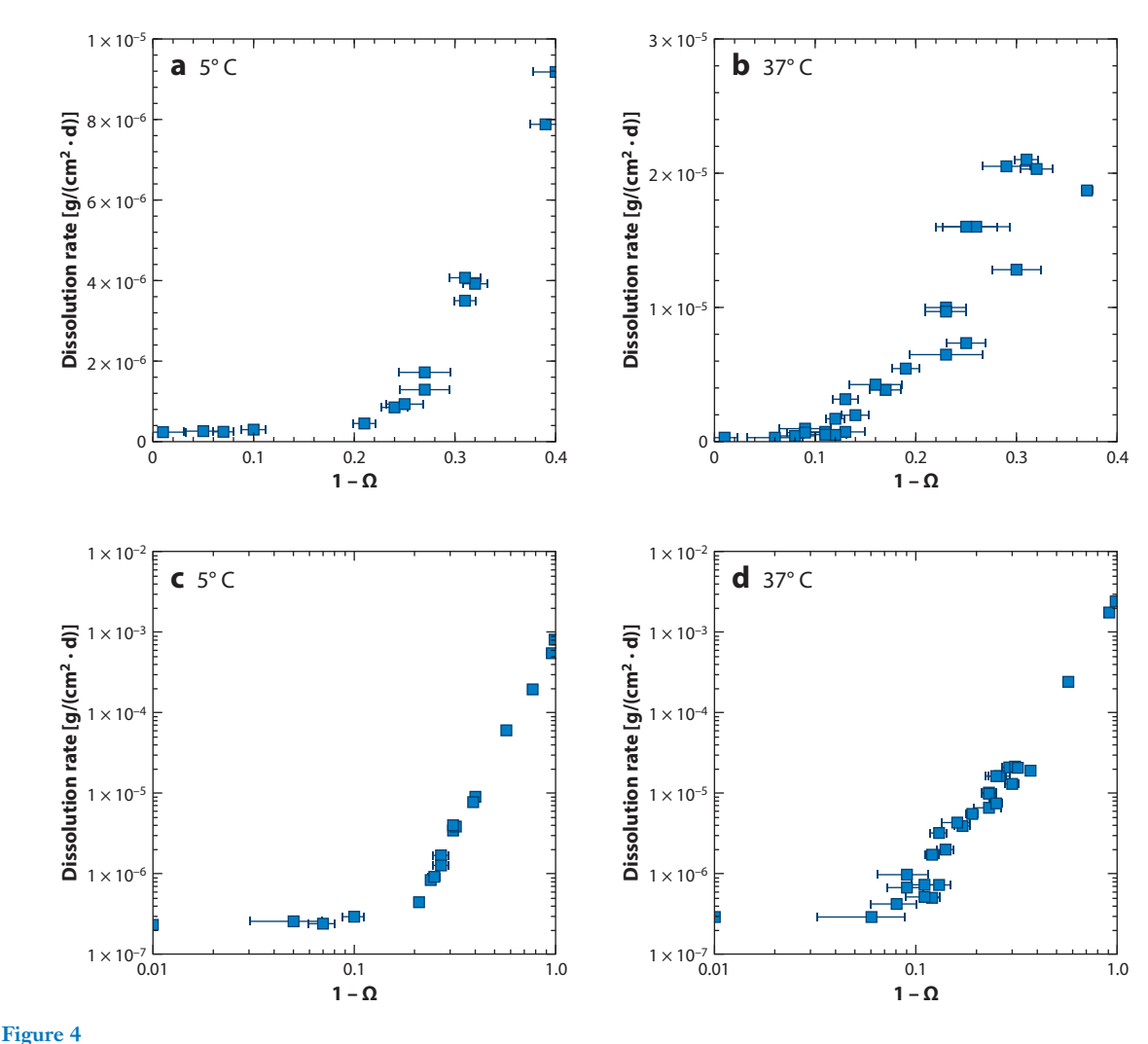


Figure 3

Raw  $\delta^{13}$ C-versus-time data for bag experiments at four different saturation states. Larger undersaturation states show faster dissolution rates. The two experiments with the slowest rates are bag replicates at the same value of  $\Omega$ . Linear increases in  $\delta^{13}$ C versus time demonstrate a steady-state net dissolution rate, while curvature in the first  $\sim$ 24 h is a function of the two gross fluxes and the unique boundary conditions of our experiments. Figure adapted with permission from Subhas et al. (2015).

the time evolution of the  $^{13}$ C/ $^{12}$ C ratio of dissolved inorganic carbon (DIC) in the bag's seawater is a direct measurement of dissolution rate (**Figure 3**). The method is extremely sensitive: For a 1- $\mu$ mol/kg change in the experimental bag's alkalinity, there is a 20% change in the  $\delta^{13}$ C. Given that we can measure this value to  $\pm 0.1\%$  on a Picarro cavity ring-down spectrometer, this method is more than 200 times more sensitive than the best alkalinity titrations. It is also more than 20 times more sensitive than Morse's pH-stat approach, with pH controlled to  $\pm 0.002$  units. The method is sensitive enough that experiments lasting a few days give robust signals, with no change in the solution  $\Omega$  value or in the surface area of the reacting solid even in this free-drift mode.

Data both near and far from saturation for inorganic calcite crystals show strong curvature in the rate law (**Figure 4**). We are able to generate data very close to equilibrium at a variety of temperatures (Naviaux et al. 2019b). When the data are plotted with linear axes, it is clear that, at the same saturation state, dissolution occurs faster at warmer temperatures than at cold temperatures. It is also clear that for all temperatures that span the relevant range in seawater, the rate laws are strongly curved. When not complicated by the mass transfer rates from sediment to bottom waters, so that we are measuring the inherent solid surface dissolution rate, the rate law is nonlinear with respect to  $\Omega$ . Plotting the same data in log-log space shows that the fits of k and n are themselves dependent on the  $\Omega$  range used in the experiment. While the Keir formulation is convenient for inclusion in models, it is not a mechanistic description of the controls on calcite dissolution in seawater. There are clear kinks in the relationship between rate and saturation state, and the first of these transitions occurs in a region directly relevant for the real ocean both in temperature and saturation state. Like the difference between fresh water and seawater shown above, these kinks also imply that saturation state alone may not be a sufficient description of the true dissolution rate law.



Dissolution rate of inorganic calcite grains as a function of the degree of undersaturation  $(1 - \Omega)$  and as a function of temperature. Data for 5°C (panels a and c) are representative of most of the ocean where waters are undersaturated. Data for 37°C (panels b and d) are the warmest experiments we have measured for seawater. Panels a and b are linear plots of the same data as the log–log plots in panels c and d. Kinks in the data are evident at  $1 - \Omega$  values of  $\sim$ 0.1 and  $\sim$ 0.25, with the cold waters skipping the 0.1 kink. Figure adapted with permission from Naviaux et al. (2019b).

Besides temperature, the isotope-labeling approach has revealed several new aspects of the dissolution rate behavior in seawater relative to the thermodynamic controls of saturation state and pressure. The curvature seen in the first 24 h of our raw data (**Figure 3**) is a function of the unique initial conditions in our experimental setup. At first, the solid is pure <sup>13</sup>C and the bulk solution is nearly pure <sup>12</sup>C (DIC is naturally only ~1.1% <sup>13</sup>C). Our experiments are always net dissolving CaCO<sub>3</sub>, but the gross forward (dissolution) and backward (precipitation) fluxes are happening at the same time. At the initiation of our experiments, the first gross dissolution flux adds pure <sup>13</sup>C to the solution above the solid, and the first gross precipitation back reaction adds nearly pure <sup>12</sup>C back to the solid surface. It is only after approximately 24 h that a steady-state

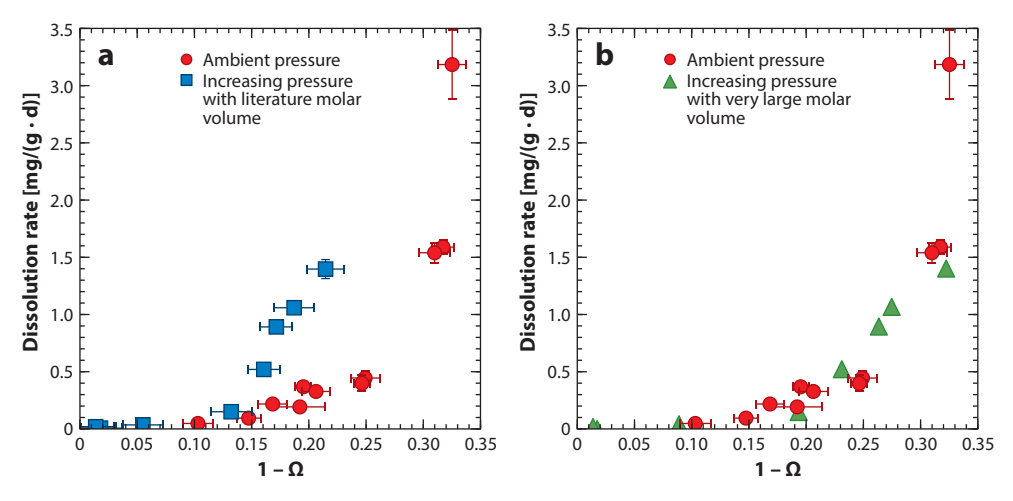


Figure 5

The pressure dependence of the calcite dissolution rate. (a) Rates from ambient pressure (*circles*) and increasing pressure (*squares*), up to 1,600 psi at the highest values. All  $\Omega$  data in this panel were calculated using the accepted specific molar volume of -37.6 cm<sup>3</sup> (Ingle 1975). (b) Ambient pressure (*circles*) and increasing pressure with a modified specific molar volume of 64 cm<sup>3</sup> (*triangles*). Adjusting the molar volume to match the ambient data requires a change that is far outside the uncertainty of the pressure dependence of the  $K_{\rm Sp}$ . Figure adapted with permission from Dong et al. (2018).

 $^{13}$ C/ $^{12}$ C ratio of the dissolving solid is established (**Figure 3**). This interplay between gross fluxes early in the experiment is the reason for the raw data's initial curvature, and the degree of this curvature is a constraint on the magnitude of the gross fluxes themselves. Compiling curve fits for all the raw data in our original publication (Subhas et al. 2015) showed that both gross fluxes are a function of the saturation state (Subhas et al. 2017). This is not surprising for the back reaction, where a Ca ion and a CO<sub>3</sub> ion have to join to form a new unit cell in the solid. However, if the standard assumption of a surface having an activity of 1 in aqueous reactions is used for CaCO<sub>3</sub> dissolution, then there should be no Ω dependence of the gross forward dissolution rate. Indeed, the lack of change in gross dissolution with Ω has been demonstrated for freshwater experiments (Arakaki & Mucci 1995). For seawater, one interpretation of this behavior is that the solid activity is not 1, but instead is a function of saturation state itself—yet another example of how a simple dependence on saturation state does not explain the dissolution kinetics.

A final twist on thermodynamic control comes from our new data on the pressure dependence of dissolution rate. **Figure 5** shows a strong pressure dependence for the dissolution rate of calcite over and above the effect of pressure on the saturation constant itself (Dong et al. 2018). We see large increases in rate with increasing pressure, up to approximately 1,600 psi, or approximately 1,100-m water depth equivalent. To make the ambient- and higher-pressure experiments fall on the same curve, we would need to change the specific molar volume of calcite from  $-37.6 \text{ cm}^3$  (Ingle 1975) to approximately  $-64 \text{ cm}^3$ . The existing estimates for this pressure dependence of the saturation constant are much tighter than this nearly  $2 \times$  offset. Pressure affects the kinetics of calcite dissolution over and above its effect on the  $K_{\rm sp}$  alone, though we do not yet understand why.

Our new approach has received some criticism for being biased by isotope exchange with no net dissolution. Indeed, long-term experiments with labeled grains in supersaturated bags show an increase in the  $\delta^{13}$ C of DIC of 1–2‰. A simple box model of the exchange process, the same one

used to generate the gross dissolution flux estimates, demonstrates that this observed enrichment is consistent with the divergent initial conditions of pure  $^{13}$ C in the solution DIC at the start of the experiment. Our measured total change over several days to a week is more than tens of per mil, and the isotope exchange fluxes do not affect the measured slopes of  $^{13}$ C dissolved versus time (**Figure 3**). While we can resolve and utilize the effect of isotope exchange due to our pure  $^{13}$ C starting material, it has no bearing on our measured slopes of  $^{13}$ C dissolved versus time at steady state.

### FORMULATING A MECHANISTIC RATE LAW FOR CALCITE IN SEAWATER

The kinks seen in rate laws for inorganic carbonate dissolution (Dong et al. 2019, Naviaux et al. 2019b, Subhas et al. 2017) (Figure 4) are indicative of an abrupt change in dissolution mode or mechanism. At nearly all temperatures and pressures we have examined, there are two critical values of  $\Omega$  where these rate relationships change dramatically. One is close to equilibrium, at approximately 0.9, although this dramatic change is not apparent in the lowest-temperature experiments and is the most difficult to constrain because the data density is not as good as that of other regions. A second abrupt shift occurs at approximately  $\Omega = 0.75$ . Generating high-resolution data at a wide range of  $\Omega$  values makes it possible to see the coherent behavior of calcite dissolution. These transitions in the rate of mineral dissolution have been recognized as the manifestation of classic crystal growth theory, based on the energetics of surface sites, but reversed to explain dissolution instead (Dove et al. 2005, Teng 2004). The basics are straightforward to understand, and they apply to all minerals that undergo congruent dissolution. Close to equilibrium, there is not enough free energy in the solution to remove solid species except at sites that are already well exposed to the solution. These steps and kinks are the first to dissolve as the saturation state moves from supersaturated to undersaturated (**Figure 6**). As  $\Omega$  drops further, vacancy sites, or etch pits, can be nucleated at the surface, but only at regions of locally high surface energy, such as sites of impurity atoms and crystal defects. Finally, when the solution is highly undersaturated, there is enough free energy available to nucleate etch pits on the planar 2-D surface without the aid of crystal defects.

There is some confusion in the literature around nomenclature here. Step edge retreat, the lowest-energy mechanism, is most commonly studied at screw dislocation defects and is well described by the classic Burton–Cabrera–Frank (BCF) theory for crystal growth (Burton et al. 1951,

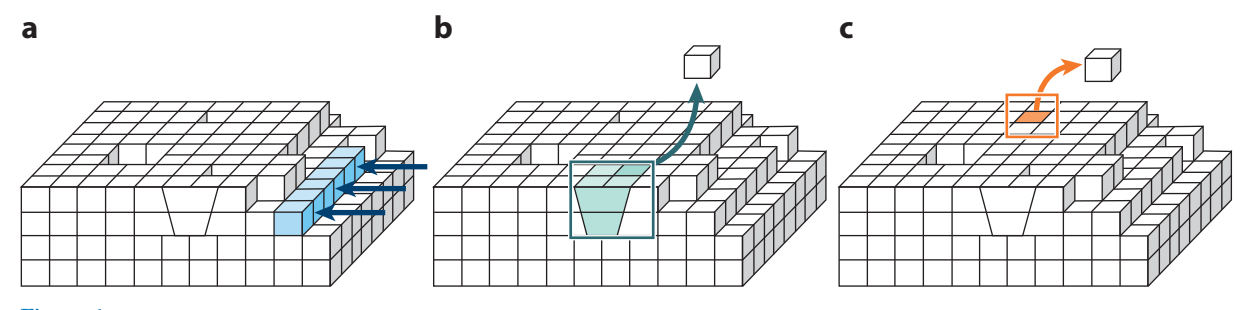


Figure 6

Schematic representation of the three dissolution modes based on surface energetic arguments. (a) Close-to-equilibrium dissolution occurs only at preexisting steps, which can come from crystal edges or screw defects. (b) After a critical threshold in solution free energy  $(\Omega_{crit})$  is crossed, etch pits can form at defects and impurities in the solid. (c) Far from equilibrium, there is enough free energy in the understaturated solution to overcome the kinetic energy barrier to 2-D etch pit formation.

Lasaga 1998). Presumably this is a dominant process in natural marine crystals, as most of the ocean's water column is close to equilibrium. The first appearance of etch pits occurs at mineral impurities or other regions of irregular ordering. Sometimes these sites are also referred to as defect assisted, but we do not mean to confuse this process with step edge retreat at screw defects. Finally, the solution can be so undersaturated that free energy is available to nucleate etch pits homogeneously across the surface—so-called 2-D etch pits. These levels of deep undersaturation can lead to rapid removal of sheets of mineral, as observed in vertical scanning interferometry (VSI) and codified into the step wave theory (Lasaga & Luttge 2001) by laboratory studies of aluminosilicates.

The advent and advancement of atomic force microscopy (AFM) allowed the mineral dissolution field to link theories of surface mechanisms to observations of dissolution rate (Arvidson et al. 2003, Hillner et al. 1992, Stipp et al. 1994). Before this unprecedented view of the dissolving surface, theory could be tested only with dissolution rate measurements based on monitoring the bulk solution evolution. In a sense, our isotope-labeling method is a return to this old way of constraining the fundamental rate law for dissolution. However, the increased sensitivity and precision of the tracer-based method allows us to compare bulk rates with surface theories in a manner not previously recognized (Luttge et al. 2013). This section of the review takes some of the pioneering work developed for the theory in Kossel crystals and begins to apply it to CaCO<sub>3</sub> dissolution (an AB crystal) in marine settings. Using quartz dissolution as an example, Dove et al. (2005) developed the equations for extracting three key parameters that control dissolution rates when surface energetics are theorized to dominate the rate law: the surface energy, the site nucleation rate, and the kinetic rate coefficient. This derivation has been worked out before (Dove et al. 2005; Lasaga 1998; Lasaga & Blum 1986; Zhang & Nancollas 1998, 1990), but we cover some of the basics here to show the theoretical origins of our fits of seawater dissolution rates and where there might be differences from the freshwater work done to date.

The fundamental description of dissolution rate is

rate = 
$$vh/\lambda$$
, 2.

where v is the velocity of a retreating step, b is the height of a unit cell of a mineral, and  $\lambda$  is the spacing of steps on its surface. For Kossel crystals, such as quartz, the velocity is a linear function of the bulk solution saturation state (Malkin et al. 1989, Zhang & Nancollas 1990):

$$v = \omega C_{\text{eq}} \beta \sigma = \omega C_{\text{eq}} \beta (\Omega - 1),$$
 3.

where  $\omega$  is the unit cell volume,  $C_{\rm eq}$  is the saturation value of the mineral,  $\sigma$  is the saturation state  $[(C-C_{\rm eq})/C_{\rm eq}]$ , and  $\beta$  is the kinetic coefficient, essentially a proportionality constant with units of velocity. This linearity arises because the rates of attachment and detachment are both functions of the chemical potential between surface and solution (Qiu & Orme 2008), which can have only one value for a Kossel solid. In an AB crystal, such as calcite, the cation and anion can have very different chemical potentials, and the dissolution rate can be dependent on the ratio A:B in solution as well as their ion product (Nielsen et al. 2012, Stack & Grantham 2010, Zhang & Nancollas 1998). This separate behavior of attachment and detachment frequencies can lead to nonlinear changes in step velocity with  $\Omega$ , especially for calcite in seawater, where the Ca ion is 10-100 times more concentrated than the CO<sub>3</sub> ion (Dong et al. 2020). The step spacing term,  $\lambda$ , is strongly dependent on the mode of surface removal, and the transitions between modes can be described as critical  $\Delta G$  values. For the transition from step edge retreat to defect-assisted etch pit formation, the free energy change of the system is the sum of the bulk dissolution reaction  $\Delta G$ , the surface energy ( $\sigma$  in some treatments,  $\sigma$  in Dove et al. 2005) multiplied by the area removed, and the strain energy of the defect site. Minimizing this  $\Delta G$  of the system leads to a critical  $\Delta G$ 

for the transition to etch pits (Lasaga & Blum 1986):

$$\Delta G_{\rm crit}^{\rm d} = \frac{2\pi^2 \alpha^2 \omega}{\mu b^2}.$$

Here, the surface energy ( $\alpha$ ) is balanced against the bulk sheer modulus ( $\mu$ ) and Burgers vector (b) of the defect. This height of the energy barrier to etch pit nucleation at defects is dependent on fundamental aspects of the solid. Homogeneous, or 2-D, etch pit formation on a flat surface, on the other hand, is directly dependent on the solution saturation state itself (Malkin et al. 1989):

$$\Delta G_{\text{crit}}^{\text{n}} = \frac{2\pi\alpha^2\omega h}{kT\ln\Omega}.$$
 5.

At first, the free energy available from the solution is not large enough for free etch pit activation compared with Equation 4, but as  $\Omega$  drops far from equilibrium, this mechanism takes over from etch pit formation at local sources of stress in the mineral.

Dove et al. (2005) used Equations 2 and 3 and a description of the step spacing based on screw dislocations to derive a predicted rate law for near-equilibrium dissolution by step edge retreat. They also used the classic formulation of the etch pit dissolution rate,  $R = hv^{2/3}J^{1/3}$  (Chernov 1984), and the frequency of pit formation, J (Malkin et al. 1989),

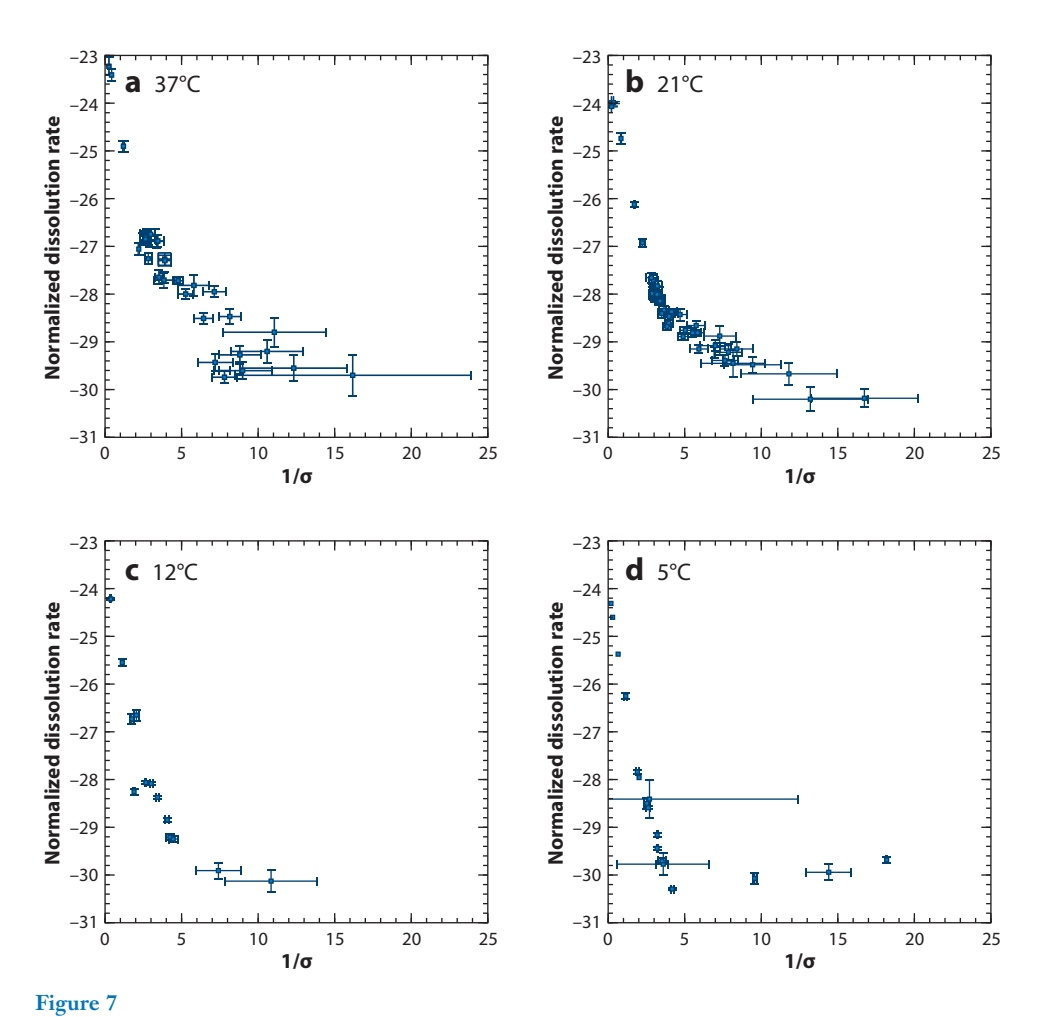
$$J = \sigma^{1/2} n_{s} a h C_{eq} \beta e^{\frac{-\pi a^{2} b}{(kT)^{2}} \left(\frac{1}{\sigma}\right)},$$
 6.

to derive the rate law further from equilibrium. Here, a is the lattice spacing and  $\sigma = \ln \Omega$ . The key new parameter, in addition to  $\beta$  and  $\alpha$ , is the density of nucleation sites  $(n_s)$  for etch pits on the free surface. The natural log of  $n_s$  is proportional to the kinetic energy barrier to the formation of etch pits on the surface layer. According to this theory, the three key terms (along with the geometry of the crystal and the saturation state)—the kinetic step coefficient  $(\beta)$ , the surface energy  $(\alpha)$ , and the spread of nucleation sites across the surface  $(n_s)$ —determine the rate of etch pit dissolution:

$$\ln\left[\frac{R_n}{(1-\Omega)^{2/3}|\sigma|^{1/6}}\right] = \ln\left[h\beta C_e(\omega^2 h n_s a)^{1/3}\right] - \frac{\pi\alpha^2\omega h}{3(k_b T)^2} \left|\frac{1}{\sigma}\right|.$$
 7.

The left-hand side of this equation, the normalized measured rate, is the y axis of a linear plot versus  $1/\sigma$ . While the equation might seem overly complicated, the slope of the dissolution rate data in this space determines the surface energy of a mineral, and the intercept is a function of  $\beta$  and  $n_s$ . In **Figure 7**, we reformulate the temperature dependence of our seawater calcite dissolution rates from **Figure 4** in this new space and add data from 12°C and 21°C. Close to equilibrium, the rate is described by a curve (equation not shown) that describes dissolution by step edge retreat. The transitions between modes are now clear and seem to happen at essentially the same  $\Omega_{\rm crit}$  regardless of temperature. The one exception to this observation is the lack of defect-assisted etch pit formation at 5°C. Here, step edge retreat dominates up to the transition to 2-D etch pit formation.

The Dove et al. (2005) formulation predicts a linear relationship between the measured slopes and  $1/T^2$  that is driven by the  $\omega$  value (the last term in Equation 7). We can extract these slopes from our data (**Figure 7**) and fit the temperature dependence for the calcite surface energy in seawater (**Figure 8**). For dissolution far from equilibrium, where etch pits are forming freely on the mineral surface, the data are consistent with a surface energy of 35.5 mJ/m² (Naviaux et al. 2019b). This value is approximately one-third of the energy determined for calcite in fresh water (Lasaga 1998, Steefel & Van Cappellen 1990). Clearly, the complicated ionic interactions in seawater are lowering the energy barrier to 2-D etch pit formation. For defect-assisted etch pit formation, the



Calcite dissolution rates as a function of saturation state at four different temperatures but plotted in the Dove et al. (2005) framework for fitting data to the surface energy. These data are the same as those in **Figure 4** but with two new temperatures added, showing (a)  $37^{\circ}$ C, (b)  $21^{\circ}$ C, (c)  $12^{\circ}$ C, and (d)  $5^{\circ}$ C. The critical values of  $\Omega$  for the dissolution mode transition appear as kinks in this plot. The slopes from the first two dissolution modes are reported in **Figure 8**. Figure adapted with permission from Naviaux et al. (2019b).

data tell a very different story. The theory embodied in Equation 7 is not even predicting the sign of the observed temperature dependence of the slopes correctly (**Figure 8**). However, the slope term contains parameters that should be constant between dissolution modes (crystal geometry, step height, the Boltzmann constant, etc.) and the surface energy ( $\omega$ ), so how can the two temperature dependencies be so different? The problem probably arises from the assumption of a linear dependence of step velocity on saturation state (Equation 3). This term is what gives rise to the  $(1 - \Omega)^{2/3}$  normalization of the measured rates on the y axis of **Figure 7**. If this normalization of the measured rates has the incorrect dependence on saturation state, then our temperature dependence will not constrain the surface energy. This misfit was one of our first clues that a rate law for calcite dissolution in seawater that was only described by surface energetics might be incomplete (see below).

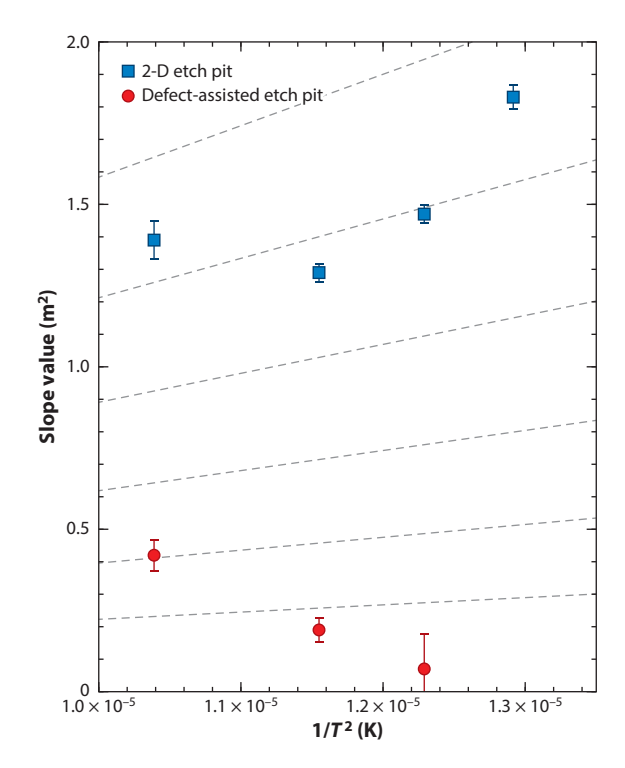


Figure 8

Slope of the dissolution rate data from **Figure 7** for the 2-D etch pit (*squares*) and defect-assisted etch pit (*circles*) regions of saturation state. The slope value is a function of the solid's surface energy and several constants related to the crystal's shape (Equation 7). The dashed gray lines show the temperature relationships expected for values of  $\alpha$  (surface energy), ranging from 15 mJ/m² to 40 mJ/m² in increments of 5 mJ/m². The 2-D etch pits fit a surface energy of  $\sim$ 34 mJ/m², but defect-assisted etch pits have the wrong slope with  $1/T^2$ . These observations clearly do not fit the surface energetic theory developed by Dove et al. (2005) for quartz dissolution in fresh water. Figure adapted with permission from Naviaux et al. (2019b).

AFM measurements of the dissolving calcite surface in fresh water have clearly demonstrated the change in etch pit type and density associated with the two critical transitions (Teng 2004, Xu et al. 2012). Like the work on quartz dissolution, this early work on calcite began to describe dissolution in the same energetic terms as classic crystal growth. However, AFM data have only recently been collected in seawater (Dong et al. 2020). Generating data over a range of  $\Omega$  values requires the control of head space  $CO_2$  inside the AFM chamber. Dong et al. (2020) constructed a system that kept the saturation state constant and monitored dissolution at steady-state conditions (**Figure 9**). Their measured etch pit densities can be compared with the bulk solution  $\Omega_{crit}$  values from Naviaux et al. (2019b). Both the bulk solution data and the direct observation of etch pit density show the same critical transitions. In each case, the transition occurs at a higher value of  $\Omega$  than it does in fresh water (**Figure 9**). These shifts in  $\Omega_{crit}$  are consistent with a lower surface energy of calcite in seawater than in fresh water and point to an important role for the activity of surface sites in setting dissolution rates.

Indeed, it was only after van Cappellen et al. (1993) determined the surface speciation of calcite in fresh water that Arakaki & Mucci (1995) were able to unify the existing bulk solution dissolution rate for fresh water into a complete rate law that explained both the dependence on proton activity and pCO<sub>2</sub> in laboratory experiments. The latter authors proposed the following four elementary

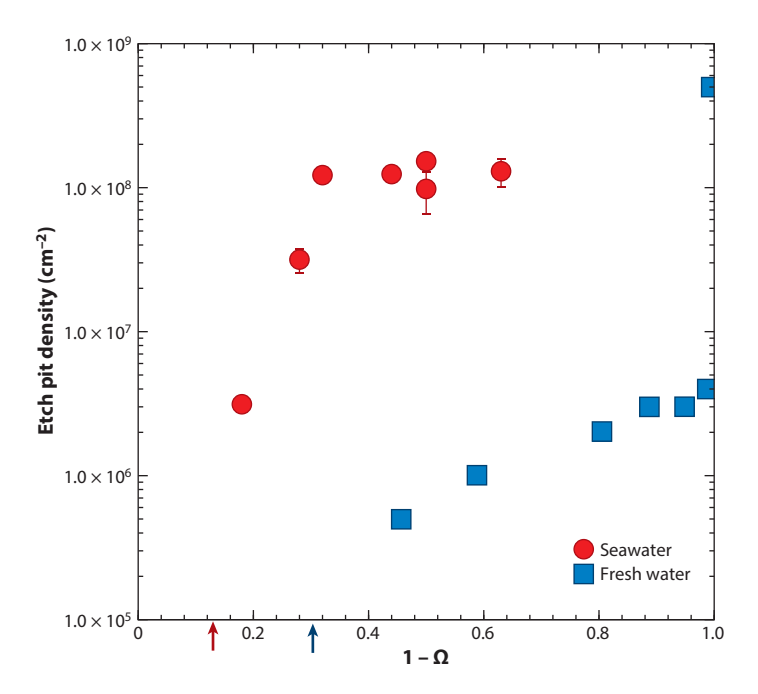


Figure 9

Etch pit density on calcite surfaces in seawater (*circles*) and fresh water (*squares*) across a range of saturation states, as measured by atomic force microscopy (AFM) (Dong et al. 2020, Teng 2004). Very far from equilibrium, both seawater and freshwater surfaces show high pit density and the formation of 2-D etch pits. Very close to equilibrium, the arrows along the x axis show where each water type had zero etch pits measured by AFM (seawater in red and fresh water in blue). For a wide range of intermediate  $\Omega$  values, calcites in fresh water are able to form etch pits only at defects, while calcite in seawater is already forming 2-D etch pits. These data point to very different surface energies for calcite in the two water types.

reactions as a complete rate law for calcite dissolution in waters with low ionic strength:

$$>CO_3^- + 2H^+ \underset{k_5}{\overset{k_1}{\rightleftarrows}} > Ca^+ + H_2CO_3,$$
 8.

$$>Ca^{+} + H_{2}CO_{3} \underset{k_{6}}{\overset{k_{2}}{\rightleftharpoons}} >CO_{3}H + CaHCO_{3}^{+},$$
 9.

$$>CO_3H + CaHCO_3^+ \underset{k_7}{\overset{k_3}{\rightleftharpoons}} >Ca^+ + H_2CO_3 + CaCO_3^0,$$
 10.

$$CaCO_{3(solid)} \underset{k_8}{\overset{k_4}{\rightleftharpoons}} CaCO_3^0.$$
 11.

This system describes the attack of the surface by  $H^+$  and  $H_2CO_3$  at  $>CO_3$  and >Ca sites, respectively, as well as general  $H_2O$  attack everywhere along the surface (Equation 11). In this scheme, the acidic ligands ( $H^+$  and  $H_2CO_3$ ) that actually attack the surface and promote dissolution need an open >Ca or  $>CO_3$  site to remove half of the AB crystal. These reactions require an understanding of the activity of free cation and anion sites on the surface, which will be very different in seawater than in fresh water. Just as van Cappellen et al. (1993) did for the freshwater work, if

we could know the activity of free surface sites in seawater, we could test this set of elementary reactions for marine calcite dissolution as well. However, one curiosity is that the Arakaki & Mucci (1995) set of elementary reactions successfully describe the freshwater dissolution rates without considering any of the energetic modes of dissolution that we have found to be important for seawater. An examination of the  $\Omega_{crit}$  values for freshwater (**Figure 9**) shows that virtually all of the bulk dissolution freshwater studies were done in the defect-assisted etch pit formation region of saturation state space. The formation of 2-D etch pits occurs at  $\Omega \sim 0.007$  (Teng 2004), and the transition to step edge retreat occurs at  $\Omega \sim 0.7$ . This is the range where most of the bulk dissolution data were collected, so most studies did not find the sharp transitions in rate characteristic of a surface mode switch.

Fortunately, several groups have determined the activity of surface sites on calcite in seawater-like solutions (Ding & Rahman 2018, Song et al. 2017), though they do not agree in some important details. With this relatively new information, one way forward on this problem is to systematically change the ionic composition of seawater while measuring the dissolution rate. This approach has proven successful in the study of individual ions within solutions that otherwise have low ionic strength (Arvidson et al. 2006, Klasa et al. 2013, Lea et al. 2001, Ruiz-Agudo et al. 2009, Vinson & Luttge 2005, Vinson et al. 2007), but both the aqueous and surface complexation in seawater are important to the problem.  $SO_4$  and  $CO_3$  will compete to form surface ion pairs with >Ca, and Ca and Mg will make surface complexes with >CO $_3$ . In addition, since only approximately 10% of the total  $CO_3$  in marine systems is not complexed by Mg into a neutral ion pair, and [Ca] is approximately 10.3 mM in the modern ocean, changing either of these ions in solution will also change the value of  $\Omega$  itself. Changing one complexing ion without the others present is not likely to capture the true behavior of seawater or to provide insight into dissolution under conditions in the past with different major ion ratios in the ocean (Hain et al. 2015, Tyrrell & Zeebe 2004).

As a first pass at this problem, we constructed synthetic seawater (Morel et al. 1979) with variable amounts of SO<sub>4</sub> but the modern concentrations of the other major cations and anions. In agreement with previous work (Sjoberg 1978), SO<sub>4</sub> acts as a dissolution rate inhibitor far from equilibrium (Figure 10). Here the reasoning is straightforward: At the modern seawater [SO<sub>4</sub>] of 28 mM, enough of the free >Ca sites are complexed that the forward reaction of Equation 9 is inhibited. However, close to equilibrium, removing SO<sub>4</sub> from seawater changes the sign of the effect and slows dissolution by an order of magnitude (diamonds in Figure 10, as on both sides of the reference rates of the squares). We can understand this behavior as a series of competitive equilibria for the complexation of the free > Ca site. In seawater, the binding constant for CO<sub>3</sub> is higher than that of SO<sub>4</sub> on the calcite surface (Ding & Rahman 2018, Song et al. 2017). However,  $[SO_4]$  is 10 times higher than the total DIC concentration and anywhere from  $\sim 20-100$ times higher than  $[CO_3]$ , depending on the value of  $\Omega$ . Thus, far from equilibrium, where  $[CO_3]$ is low enough, SO<sub>4</sub> complexes the calcite surface and slows the dissolution rate by lowering the activity of free Ca sites. If SO<sub>4</sub> is taken away from these relatively acidic solutions, then the dissolution rate increases (Figure 10). But close to equilibrium, [CO<sub>3</sub>] is high enough to compete with SO<sub>4</sub> for >Ca sites. As it is more strongly bound to the surface, this CO<sub>3</sub> ion complex slows dissolution more than a SO<sub>4</sub>-bound site because it is harder for the acidic ligands to displace the CO<sub>3</sub>-complexed surface site. In the presence of SO<sub>4</sub>, the activity of CO<sub>3</sub>-bound sites is lower due to the competitive equilibrium and the high [SO<sub>4</sub>], and so the overall dissolution rate is higher. When SO<sub>4</sub> is not present in seawater, more of the >Ca sites are complexed by the strongly bound CO<sub>3</sub> ion, and dissolution slows down. In a first attempt to quantify this effect, Naviaux (2019) was able to use the Arakaki & Mucci (1995) elementary equations to fit the zero, one-half, and full [SO<sub>4</sub>] data in synthetic seawater. The offset between the squares, triangles, and diamonds

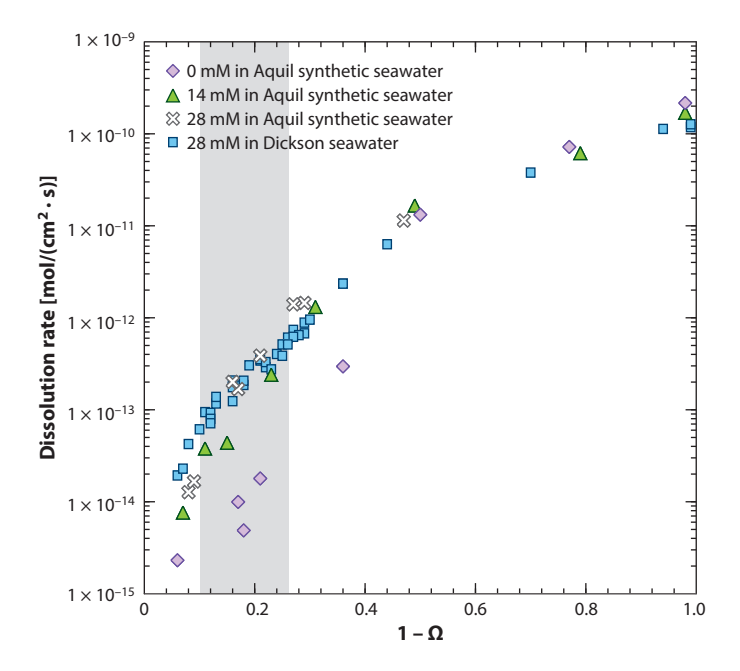


Figure 10

Calcite dissolution rates in the laboratory with different  $SO_4$  concentrations: 0 mM in Aquil synthetic seawater (diamonds), 14 mM in Aquil synthetic seawater (triangles), and 28 mM in Dickson standard seawater (squares). The crosses represent Aquil synthetic seawater with a full complement of  $SO_4$  at 28 mM and lie on top of the Dickson seawater data. The range of defect-assisted etch pit formation is shown as a gray rectangle (roughly  $0.75 < \Omega < 0.9$ ). Figure adapted from Naviaux (2019).

in **Figure 10** can be explained by the changing activities of the surface sites in Equations 8–10, with the same rate constants for all three cases. This rate law works only in the defect-assisted etch pit mode of dissolution (gray rectangle in **Figure 10**), where the freshwater mechanism was initially fit, and requires much smaller rate constants in seawater compared with fresh water.

The new bulk dissolution data with the sensitive  $^{13}$ C method makes it clear that calcite dissolution in seawater requires both surface energetic and aqueous complexation components to fully explain the rate-versus-saturation-state relationship. We now understand that the curvature in the rate law, when described as a curve fit with a reaction rate (k) and a reaction order (n), is a result of different modes of dissolution at different values of undersaturation. The effect of these critical  $\Omega$  values is to make the value of n change as a function of  $\Omega$  and can explain why so many empirical rate laws populate the literature (**Figure 2**). While the insight of Morse and Berner (Berner & Morse 1974, Morse & Berner 1972) was on the right path, their attribution of surface poisoning by  $PO_4$  ions turns out not to be correct. These modes are controlled by the surface energy land-scape of  $CaCO_3$  in seawater with the chemical complexation of the surface yielding very different transition points than seen in fresh water. Yet, while the system is fundamentally set by surface energetics, dissolution rates in seawater are also controlled by the same three elementary reactions proposed by Arakaki & Mucci (1995) for freshwater data. For now, this appears to be true only for defect-assisted etch pit formation, but we are on the path to convergence between systems that have been thought to be widely divergent.

### BACK TO CHEMICAL OCEANOGRAPHY

With a better understanding of the controls on the calcite dissolution rate law in seawater, it is useful to return to how this detailed physical chemistry might matter for various aspects of ocean chemistry. To address this issue and more directly compare in situ rates with our laboratory-based results, we built and deployed specialized reactors to measure the CaCO<sub>3</sub> dissolution rate in the water column (Naviaux et al. 2019a). Like our gas-impermeable bags for the laboratory, the modified Niskin bottles are a closed system with an external pump that circulates ambient seawater around  $^{13}$ C-labeled grains. The bottles incubate on a wire for 12–36 h, and the difference in  $\delta^{13}$ C before and after the experiment is a direct measure of the dissolution rate. Our data for inorganic calcite grains from a CDISK4 transect from Hawaii to Alaska are shown in **Figure 11** (blue squares); the in situ data show the same shape, with the same  $\Omega_{\rm crit}$ , as our 5°C laboratory data (red circles). While the ocean samples are approximately four times slower than the benchtop rates, they clearly both show the transition from step edge retreat to etch pit formation. The laboratory data and the in situ data are showing the same mechanistic control of calcite dissolution in seawater as the field has already demonstrated for fresh water.

We used the Global Ocean Data Analysis Project (GLODAP) database to calculate  $\Omega$  at each of the depths of the Peterson (1966) array of calcite spheres (**Figure 1**). These 50-year-old data (small black squares in **Figure 11**) compare well with the laboratory and in situ data. Peterson's rapid jump in dissolution rate at  $\sim$ 3,500 m is a switch in the surface mode of dissolution. This switch results not so much from the masking and coating of his spherical surfaces (unless he meant the lowering of the surface energy) as from the formation of etch pits on the surfaces of the samples

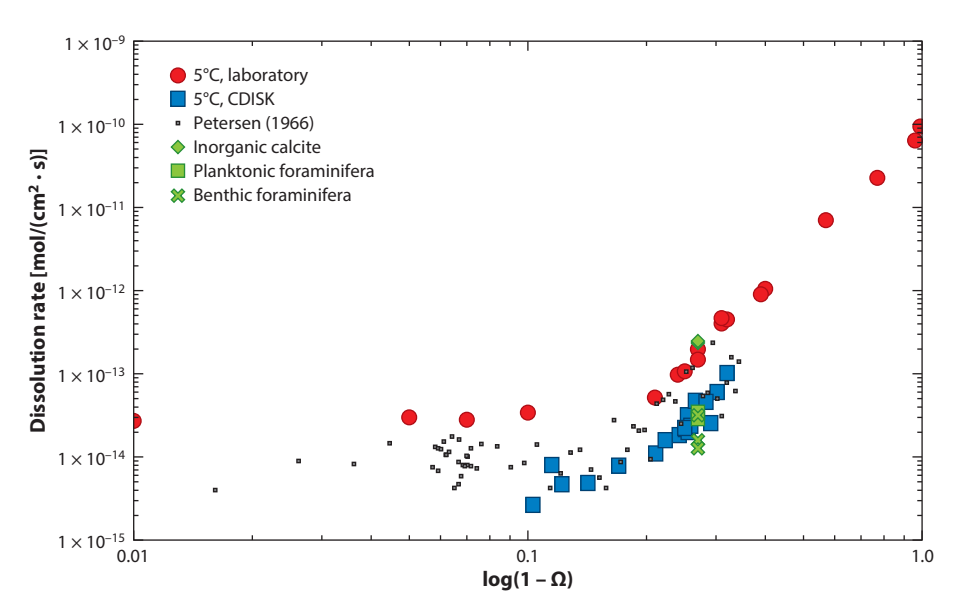


Figure 11

Calcite dissolution rates in the laboratory and in the ocean, showing 5°C data collected in the laboratory (red circles) (Naviaux et al. 2019b) and during a North Pacific transect as part of the CDISK4 cruise from Hawaii to Alaska (blue squares) (Naviaux et al. 2019a); calcite sphere data from **Figure 1** (small black squares) (Peterson 1966); and inorganic calcite data (green diamonds), planktonic foraminifera data (green squares), and benthic foraminifera data (green crosses) (Honjo & Erez 1978). All inorganic calcite data have the same kink at  $\Omega \sim 0.9$  whether they are from the laboratory or from in situ measurements. Figure adapted with permission from Naviaux et al. (2019a).

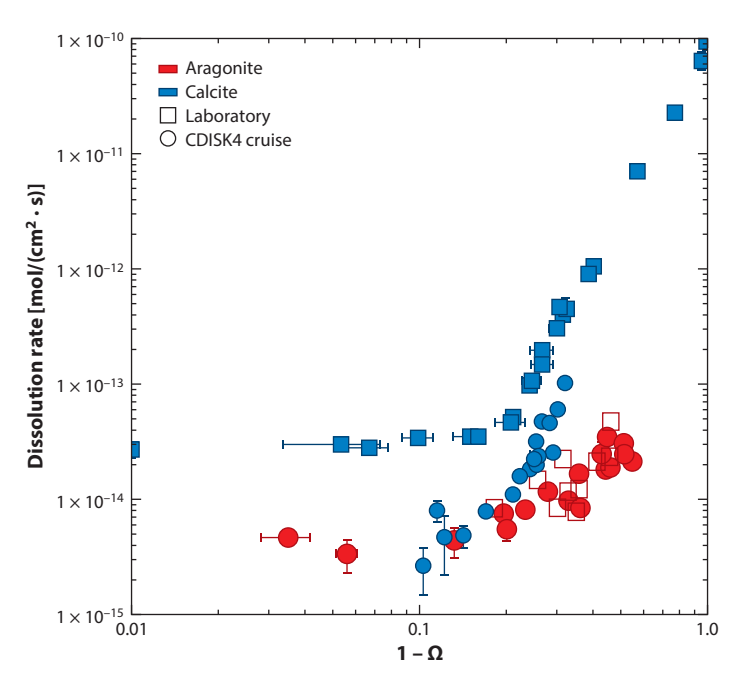


Figure 12

Aragonite and calcite dissolution rates (*red* and *blue*, respectively) at 5°C in the laboratory (*squares*) and from the North Pacific CDISK4 cruise (*circles*). Figure based on data from Dong et al. (2019) and Naviaux et al. (2019a,b).

as the water column saturation state passes through  $\Omega_{crit}$ . His careful preparation of the calcite spheres and elegant experimental procedure produced a seminal data set that is still relevant today. The quantitative consistency with Berger's (1967) foraminifera data has also been true of our recent work. Biogenic carbonates can be labeled with  $^{13}$ C during their calcification in culture and then used in the laboratory or in situ to monitor their dissolution rate (Subhas et al. 2018). While there are not nearly as many biogenic data as there are data for inorganic crystals, these materials show the same  $\Omega_{crit}$  values and fall in the range established by our 5°C laboratory data and the Niskin reactor data (not shown in **Figure 11**). And finally, the in situ work on the dissolution rates of calcite (green diamonds in **Figure 11**) and foraminifera (green squares and crosses) from Honjo & Erez (1978) also fall within the envelope of our laboratory and Niskin incubator data. There is much better agreement in the literature than has been previously assumed.

Another interesting test of the emerging theory is the dissolution rate of aragonite in seawater (Dong et al. 2019). This polymorph of CaCO<sub>3</sub> is more soluble than calcite and is produced ubiquitously in the open ocean by pteropods. We have studied it in the laboratory and on our Hawaii-to-Alaska transect (**Figure 12**). As with calcite, there is an  $\Omega_{\rm crit}$  at approximately 0.9 and a very low-order dependence on saturation state near equilibrium. The most striking difference with calcite is the lower slope of the rate versus  $1 - \Omega$  in the defect-assisted etch pit zone. This could be due to an even lower surface energy in seawater for aragonite than calcite, but we are not yet sure of the effects from site density ( $n_s$ ) or step velocity ( $\omega$ ) to be sure of the differences. The strong agreement between laboratory and in situ rates and the similar transition from the step edge to etch pit dissolution mode give us confidence that there is convergence toward a comprehensive rate law for all CaCO<sub>3</sub> in natural waters, though more data need to be collected over a

wider range of  $\Omega$ . When combined with its higher solubility, the lower slope of aragonite dissolution with  $1 - \Omega$  means that, at a given  $[CO_3]$  in the deep ocean, the aragonite and calcite dissolution rates might cross. Calcite is normally slower to dissolve, just because it transitions from net precipitation to net dissolution later than aragonite. But once  $[CO_3]$  values drop enough to transition to defect-assisted etch pit formation, calcite rates rise much faster than aragonite rates. This feature might allow for fast-sinking pteropods to be better preserved in some sedimentary environments or at times of higher deep-water  $[CO_3]$  (Berger 1977).

#### CONCLUSIONS

The literature on carbonate dissolution in the ocean has been marked with widespread disagreement between laboratory and in situ rates, as well as between inorganic and biogenic forms. We have shown how a new, sensitive, tracer-based technique is helping to resolve these differences. Curvature in the rate is itself a function of  $\Omega$  due to three distinct modes of surface energetic control on the dissolution mechanism. Because many studies have worked far from equilibrium, these mode shifts have given rise to a variety of rate laws in the literature, but we now know that it is not possible to extrapolate far from equilibrium data to the more relevant range of saturation states in real seawater. But mode changes are not the only important contributor to the fundamental mechanism of CaCO<sub>3</sub> dissolution. Within a single mode, the nature of the chemical attack of the mineral is strongly influenced by the chemical speciation of the solution and the surface. Using the dependence on  $[SO_4]$  as one example, we have shown how the three elementary rate equations for freshwater calcite dissolution are also applicable to seawater rates in the  $\Omega$  range where etch pit formation at surface defects is the dominant dissolution mode. The early work of Petersen on calcite spheres exposed to corrosive seawater for several months captured the main features of the dissolution rate law that we recognize today. This is true for biogenic carbonates as well as inorganic crystals, though offsets in the absolute rate are possible while still preserving the shape of the rate law versus saturation state. The role of the Ca:CO3 ion ratio and the Mg/Ca content of seawater in setting the dissolution rate remain as important unresolved questions. While it is clear that transport limitation of CaCO<sub>3</sub> dissolution at the seafloor can play a role in the rate of alkalinity return to the deep ocean, the inherent chemical rate is very slow close to equilibrium. and it is likely that both physical and chemical factors limit the timescale for carbonate dissolution to drive the ocean's alkalinity to a steady state.

### **DISCLOSURE STATEMENT**

The authors are not aware of any affiliations, memberships, funding, or financial holdings that might be perceived as affecting the objectivity of this review.

### ACKNOWLEDGMENTS

We thank the National Science Foundation for its support of this research via awards OCE-1220600, OCE-1559215, OCE-1834492, OCE-1559004, OCE-1220302, and OCE-1834475. We have also benefited from financial support from the Linde Center for Global Environmental Science at Caltech, the Change Happens Foundation, and the Grantham Foundation. Little of this work would have been possible without the technical support of Nick Rollins and intellectual inspiration from Jonathan Erez. Conversations with many colleagues over the years have helped shape our understanding of carbonate dissolution kinetics, but we are especially indebted to Burke Hales and Henry Teng for insightful comments and criticisms along the way.

#### LITERATURE CITED

- Arakaki T, Mucci A. 1995. A continuous and mechanistic representation of calcite reaction-controlled kinetics in dilute solutions at 25°C and 1 atm total pressure. Aquat. Geochem. 1:105–30
- Archer D. 1991. Modeling the calcite lysocline. J. Geophys. Res. 96:17037-50
- Archer D, Emerson S, Smith C. 1989. Direct measurement of the diffusive sublayer at the deep sea floor using oxygen microelectrodes. *Nature* 340:623–26
- Archer D, Kheshgi H, Maier-Reimer E. 1998. Dynamics of fossil fuel CO<sub>2</sub> neutralization by marine CaCO<sub>3</sub>. Glob. Biogeochem. Cycles 12:259–76
- Arvidson RS, Collier M, Davis KJ, Vinson MD, Amonette JE, Lüttge A. 2006. Magnesium inhibition of calcite dissolution kinetics. Geochim. Cosmochim. Acta 70:583–94
- Arvidson RS, Ertan IE, Amonette JE, Luttge A. 2003. Variation in calcite dissolution rates: a fundamental problem? Geochim. Cosmochim. Acta 67:1623–34
- Bednaršek N, Tarling GA, Bakker DCE, Fielding S, Feely RA. 2014. Dissolution dominating calcification process in polar pteropods close to the point of aragonite undersaturation. *PLOS ONE* 9:e109183
- Bender M, Martin W, Hess J, Sayles F, Ball L, Lambert C. 1987. A whole-core squeezer for interfacial porewater sampling. *Limnol. Oceanogr.* 32:1214–25
- Ben-Yaakov S, Ruth E, Kaplan IR. 1974. Carbonate compensation depth: relation to carbonate solubility in ocean waters. *Science* 184:982–84
- Berelson WM, Balch WM, Najjar R, Feely RA, Sabine C, Lee K. 2007. Relating estimates of CaCO<sub>3</sub> production, export, and dissolution in the water column to measurements of CaCO<sub>3</sub> rain into sediment traps and dissolution on the sea floor: a revised global carbonate budget. *Glob. Biogeochem. Cycles* 21:GB1024
- Berelson WM, Hammond DE, McManus J, Kilgore TE. 1994. Dissolution kinetics of calcium-carbonate in equatorial Pacific sediments. Glob. Biogeochem. Cycles 8:219–35
- Berelson WM, Hammond DE, Smith KL, et al. 1987. In situ benthic flux measurement devices: bottom lander technology. Mar. Technol. Soc. 7. 21:26–32
- Berger WH. 1967. Foraminiferal ooze: solution at depths. Science 156:383-85
- Berger WH. 1977. Deep-sea carbonate and the deglaciation preservation spike in pteropods and foraminifera.

  Nature 269:301–4
- Berger WH, Adelseck CG, Mayer LA. 1976. Distribution of carbonate in surface sediments of the Pacific Ocean. J. Geophys. Res. Oceans 81:2617–27
- Berner RA, Morse JW. 1974. Dissolution kinetics of calcium carbonate in sea water; IV. Theory of calcite dissolution. Am. J. Sci. 274:108–34
- Biscaye PE, Kolla V, Turekian KK. 1976. Distribution of calcium carbonate in surface sediments of the Atlantic Ocean. J. Geophys. Res. Oceans 81:2595–603
- Boudreau BP. 2013. Carbonate dissolution rates at the deep ocean floor. Geophys. Res. Lett. 40:744-48
- Boudreau BP, Sulpis O, Mucci A. 2020. Control of CaCO<sub>3</sub> dissolution at the deep seafloor and its consequences. *Geochim. Cosmochim. Acta* 268:90–106
- Broecker WS, Peng T-H. 1987. The role of CaCO<sub>3</sub> compensation in the glacial to interglacial CO<sub>2</sub> change. *Glob. Biogeochem. Cycles* 1:15–29
- Broecker WS, Takahashi T. 1978. The relationship between lysocline depth and in situ carbonate ion concentration. *Deep-Sea Res.* 25:65–95
- Burton WK, Cabrera N, Frank FC. 1951. The growth of crystals and the equilibrium structure of their surfaces. Philos. Trans. R. Soc. A 243:299–358
- Busenberg E, Plummer LN. 1986. A comparative study of the dissolution and crystal growth kinetics of calcite and aragonite. In *Studies in Diagenesis*, ed. FA Mumpton, pp. 139–68. US Geol. Surv. Bulletin 1578. Washington, DC: US Geol. Surv.
- Byrne RH, Acker JG, Betzer PR, Feely RA, Cates MH. 1984. Water column dissolution of aragonite in the Pacific Ocean. *Nature* 312:321–26
- Cai W-J, Reimers CE, Shaw T. 1995. Microelectrode studies of organic carbon degradation and calcite dissolution at a California Continental rise site. Geochim. Cosmochim. Acta 59:497–511
- Chernov AA. 1984. Modern Crystallography III: Crystal Growth. Berlin: Springer

- Cubillas P, Kohler S, Prieto M, Chairat C, Oelkers EH. 2005. Experimental determination of the dissolution rates of calcite, aragonite, and bivalves. *Chem. Geol.* 216:59–77
- Ding H, Rahman SR. 2018. Investigation of the impact of potential determining ions from surface complexation modeling. *Energy Fuels* 32:9314–21
- Dong S, Berelson WM, Adkins JF, Rollins NE, Naviaux JD, et al. 2020. An atomic force microscopy study of calcite dissolution in seawater. Geochim. Cosmochim. Acta. 283:40–53
- Dong S, Berelson WM, Rollins NE, Subhas AV, Naviaux JD, et al. 2019. Aragonite dissolution kinetics and calcite/aragonite ratios in sinking and suspended particles in the North Pacific. *Earth Planet. Sci. Lett.* 515:1–12
- Dong S, Subhas AV, Rollins NE, Naviaux JD, Adkins JF, Berelson WM. 2018. A kinetic pressure effect on calcite dissolution in seawater. Geochim. Cosmochim. Acta 238:411–23
- Dove PM, Han N, De Yoreo JJ. 2005. Mechanisms of classical crystal growth theory explain quartz and silicate dissolution behavior. *PNAS* 102:10566
- Edmond JM. 1974. On the dissolution of carbonate and silicate in the deep ocean. *Deep-Sea Res. Oceanogr. Abstr.* 21:455–80
- Elderfield H, Schultz A. 1996. Mid-ocean ridge hydrothermal fluxes and the chemical composition of the ocean. *Annu. Rev. Earth Planet. Sci.* 24:191–224
- Emerson SR, Bender ML. 1981. Carbon fluxes at the sediment-water interface of the deep sea: calcium carbonate preservation. *J. Mar. Res.* 39:139–62
- Fabry VJ. 1990. Shell growth rates of pteropod and heteropod molluscs and aragonite production in the open ocean: implications for the marine carbonate system. *J. Mar. Res.* 48:209–22
- Feely RA, Sabine CL, Lee K, Berelson WM, Kleypas J, et al. 2004. Impact of anthropogenic CO<sub>2</sub> on the CaCO<sub>3</sub> system in the oceans. *Science* 305:362–66
- Feely RA, Sabine CL, Lee K, Millero FJ, Lamb MF, et al. 2002. In situ calcium carbonate dissolution in the Pacific Ocean. *Glob. Biogeochem. Cycles* 16:91-1-12
- Friis K, Najjar RG, Follows MJ, Dutkiewicz S. 2006. Possible overestimation of shallow-depth calcium carbonate dissolution in the ocean. Glob. Biogeochem. Cycles 20:GB4019
- Fukuhara T, Tanaka Y, Ioka N, Nishimura A. 2008. An in situ experiment of calcium carbonate dissolution in the central Pacific Ocean. Int. J. Greenb. Gas Control 2:78–88
- Hain M, Sigman DM, Higgins S, Haug GH. 2015. The effects of secular calcium and magnesium concentration changes on the thermodynamics of seawater acid/base chemistry: implications for Eocene and Cretaceous ocean carbon chemistry and buffering. Glob. Biogeochem. Cycles 29:517–33
- Hales B, Emerson SR. 1997. Evidence in support of first-order dissolution kinetics for calcite in seawater. Earth Planet. Sci. Lett. 148:317–27
- Hales B, Emerson SR, Archer DE. 1994. Respiration and dissolution in the sediments of the western North Atlantic: estimates from models of in situ microelectrode measurements of porewater oxygen and pH. Deep-Sea Res. 141:695-719
- Hillner PE, Gratz AJ, Manne S, Hansma PK. 1992. Atomic-scale imaging of calcite growth and dissolution rate in real time. *Geology* 20:359–62
- Honjo S, Erez J. 1978. Dissolution rates of calcium carbonate in the deep ocean; an in-situ experiment in the North Atlantic Ocean. *Earth Planet. Sci. Lett.* 40:287–300
- Ilyina T, Zeebe RE. 2012. Detection and projection of carbonate dissolution in the water column and deep-sea sediments due to ocean acidification. *Geophys. Res. Lett.* 39:L06606
- Ingle SE. 1975. Solubility of calcite in the ocean. Mar. Chem. 3:301-19
- Jahnke RA. 1990. Early diagenesis and recycling of biogenic debris at the seafloor, Santa Monica Basin, California. 7. Mar. Res. 48:413–36
- Keir RS. 1980. The dissolution kinetics of biogenic calcium carbonates in seawater. *Geochim. Cosmochim. Acta* 44:241–52
- Keir RS. 1983. Variation in the carbonate reactivity of deep-sea sediments: determination from flux experiments. Deep-Sea Res. A 30:279–96
- Klasa J, Ruiz-Agudo E, Wang LJ, Putnis CV, Valsami-Jones E, et al. 2013. An atomic force microscopy study of the dissolution of calcite in the presence of phosphate ions. *Geochim. Cosmochim. Acta* 117:115–28

- Kolla V, Be AWH, Biscaye PE. 1976. Calcium carbonate distribution in the surface sediments of the Indian Ocean. 7. Geophys. Res. Oceans 81:2605–16
- Lasaga AC. 1998. Kinetic Theory in the Earth Sciences. Princeton, NJ: Princeton Univ. Press
- Lasaga AC, Blum AE. 1986. Surface chemistry, etch pits and mineral-water reactions. Geochim. Cosmochim. Acta 50:2363–79
- Lasaga AC, Luttge A. 2001. Variation of crystal dissolution rate based on a dissolution stepwave model. Science 291:2400–4
- Lea AS, Amonette JE, Baer DR, Liang Y, Colton NG. 2001. Microscopic effects of carbonate, manganese, and strontium ions on calcite dissolution. *Geochim. Cosmochim. Acta* 65:369–79
- Luttge A, Arvidson RS, Fischer C. 2013. A stochastic treatment of crystal dissolution kinetics. *Elements* 9:183–88
- Malkin AI, Chernov AA, Alexeev IV. 1989. Growth of dipyramidal face of dislocation-free ADP crystals: free energy of steps. J. Cryst. Growth 97:765–69
- Milliman JD. 1993. Production and accumulation of calcium carbonate in the ocean: budget of a nonsteady state. Glob. Biogeochem. Cycles 7:927–57
- Milliman JD, Troy PJ, Balch WM, Adams AK, Li Y-H, MacKenzie FT. 1999. Biologically mediated dissolution of calcium carbonate above the chemical lysocline? *Deep-Sea Res. I* 46:1653–69
- Morel FMM, Rueter JG, Anderson DM, Guillard RRL. 1979. Aquil: a chemically defined phytoplankton culture medium for trace metal studies. *J. Phycol.* 15:135–41
- Morse JW. 1978. Dissolution kinetics of calcium carbonate in sea water: VI. The near equilibrium dissolution kinetics of calcium carbonate-rich deep sea sediments. *Am. 7. Sci.* 278:344–53
- Morse JW, Berner RA. 1972. Dissolution kinetics of calcium carbonate in sea water: II. A kinetic origin for the lysocline. Am. J. Sci. 272:840–51
- Mucci A. 1983. The solubility of calcite and aragonite in seawater at various salinities, temperatures, and one atmosphere total pressure. *Am. J. Sci.* 283:780–99
- Naviaux JD. 2019. Chemical and physical mechanisms of calcite dissolution in seawater. PhD Thesis, Calif. Inst. Technol., Pasadena
- Naviaux JD, Subhas AV, Dong S, Rollins NE, Liu X, et al. 2019a. Calcite dissolution rates in seawater: lab versus in-situ measurements and inhibition by organic matter. Mar. Chem. 215:103684
- Naviaux JD, Subhas AV, Rollins NE, Dong S, Berelson WM, Adkins JF. 2019b. Temperature dependence of calcite dissolution kinetics in seawater. Geochim. Cosmochim. Acta 246:363–84
- Nielsen LC, DePaolo DJ, De Yoreo JJ. 2012. Self-consistent ion-by-ion growth model for kinetic isotopic fractionation during calcite precipitation. Geochim. Cosmochim. Acta 86:166–81
- Peterson MNA. 1966. Calcite: rates of dissolution in a vertical profile in the central Pacific. Science 154:1542–44
- Qiu SR, Orme CA. 2008. Dynamics of biomineral formation at the near-molecular level. Chem. Rev. 108:4784–822
- Ruiz-Agudo E, Putnis CV, Jiménez-López C, Rodriguez-Navarro C. 2009. An atomic force microscopy study of calcite dissolution in saline solutions: the role of magnesium ions. Geochim. Cosmochim. Acta 73:3201–17
- Salter MA, Harborne AR, Perry CT, Wilson RW. 2017. Phase heterogeneity in carbonate production by marine fish influences their roles in sediment generation and the inorganic carbon cycle. Sci. Rep. 7:765
- Salter MA, Perry CT, Smith AM. 2019. Calcium carbonate production by fish in temperate marine environments. *Limnol. Oceanogr.* 64:2755–70
- Santschi PH, Anderson RF, Fleisher MQ, Bowles W. 1991. Measurements of diffusive sublayer thickness in the ocean by alabaster dissolution, and their implications for the measurements of benthic fluxes. J. Geophys. Res. 96:10641–57
- Sayles FL. 1985. CaCO<sub>3</sub> solubility in marine sediments: evidence for equilibrium and non-equilibrium behavior. Geochim. Cosmochim. Acta 49:877–88
- Sayles FL, Mangelsdorf PC, Wilson TRS, Hume DN. 1976. A sampler for the in situ collection of marine sedimentary pore waters. *Deep-Sea Res. Oceanogr. Abstr.* 23:259–64
- Sigman DM, McCorkle DC, Martin WB. 1998. The calcite lysocline as a constraint on glacial/interglacial low-latitude production changes. Glob. Biogeochem. Cycles 12:409–27

- Sjoberg EL. 1978. Kinetics and Mechanism of Calcite Dissolution in Aqueous Solutions at Low Temperatures. Stockholm: Almqvist & Wiksell
- Song J, Zeng Y, Wang L, Duan X, Puerto M, et al. 2017. Surface complexation modeling of calcite zeta potential measurements in brines with mixed potential determining ions (Ca<sup>2+</sup>, CO<sub>3</sub><sup>2-</sup>, Mg<sup>2+</sup>, SO<sub>4</sub><sup>2-</sup>) for characterizing carbonate wettability. *7. Colloid Interface Sci.* 506:169–79
- Stack A, Grantham MC. 2010. Growth rate of calcite steps as a function of aqueous calcium-to-carbonate ratio: independent attachment and detachment of calcium and carbonate ions. Cryst. Growth Des. 10:1409–13
- Steefel CI, Van Cappellen P. 1990. A new kinetic approach to modeling water-rock interaction: the role of nucleation, precursors, and Ostwald ripening. Geochim. Cosmochim. Acta 54:2657–77
- Stipp SLS, Heggleston CM, Nielsen BS. 1994. Calcite surface structure observed at microtopographic and molecular scales with atomic force microscopy. *Geochim. Cosmochim. Acta* 58:3023–33
- Subhas AV, Adkins JF, Rollins NE, Naviaux JD, Erez J, Berelson WM. 2017. Catalysis and chemical mechanisms of calcite dissolution in seawater. PNAS 114:8175–80
- Subhas AV, Rollins NE, Berelson WM, Dong S, Erez J, Adkins JF. 2015. A novel determination of calcite dissolution kinetics in seawater. Geochim. Cosmochim. Acta 170:51–68
- Subhas AV, Rollins NE, Berelson WM, Erez J, Ziveri P, et al. 2018. The dissolution behavior of biogenic calcites in seawater and a possible role for magnesium and organic carbon. *Mar. Chem.* 205:100–12
- Sulpis O, Boudreau BP, Mucci A, Jenkins C, Trossman DS, et al. 2018. Current CaCO<sub>3</sub> dissolution at the seafloor caused by anthropogenic CO<sub>2</sub>. PNAS 115:11700–5
- Sulpis O, Lix C, Mucci A, Boudreau BP. 2017. Calcite dissolution kinetics at the sediment-water interface in natural seawater. Mar. Chem. 195:70–83
- Teng HH. 2004. Controls by saturation state on etch pit formation during calcite dissolution. Geochim. Cosmochim. Acta 68:253–62
- Tyrrell T, Zeebe RE. 2004. History of carbonate ion concentration over the last 100 million years. *Geochim. Cosmochim. Acta* 68:3521–30
- van Cappellen P, Charlet L, Stumm W, Wersin P. 1993. A surface complexation model of the carbonate mineral-aqueous solution interface. *Geochim. Cosmochim. Acta* 57:3505–18
- Vinson MD, Arvidson RS, Luttge A. 2007. Kinetic inhibition of calcite (1 0 4) dissolution by aqueous manganese (II). 7. Cryst. Growth 307:116–25
- Vinson MD, Luttge A. 2005. Multiple length-scale kinetics: an integrated study of calcite dissolution rates and strontium inhibition. Am. J. Sci. 305:119–46
- Xu J, Fan C, Teng HH. 2012. Calcite dissolution kinetics in view of Gibbs free energy, dislocation density, and pCO<sub>2</sub>. Chem. Geol. 322–323:11–18
- Zhang J, Nancollas GH. 1990. Kink densities along a crystal surface step at low temperatures and under nonequilibrium conditions. *7. Cryst. Growth* 106:181–90
- Zhang J, Nancollas GH. 1998. Kink density and rate of step movement during growth and dissolution of an AB crystal in a nonstoichiometric solution. *J. Colloid Interface Sci.* 200:131–45

### Contents

Right Place, Right Time: An Informal Memoir  Carl Wunsch	. 1
Natural and Anthropogenic Drivers of Acidification in Large Estuaries  Wei-Jun Cai, Richard A. Feely, Jeremy M. Testa, Ming Li, Wiley Evans,  Simone R. Alin, Yuan-Yuan Xu, Greg Pelletier, Anise Ahmed, Dana J. Greeley,  Jan A. Newton, and Nina Bednaršek	23
The Dissolution Rate of CaCO <sub>3</sub> in the Ocean  Jess F. Adkins, John D. Naviaux, Adam V. Subhas, Sijia Dong,  and William M. Berelson  5	57
The Biogeochemistry of Marine Polysaccharides: Sources, Inventories, and Bacterial Drivers of the Carbohydrate Cycle  C. Arnosti, M. Wietz, T. Brinkhoff, JH. Hehemann, D. Probandt,  L. Zeugner, and R. Amann	31
The Complexity of Spills: The Fate of the Deepwater Horizon Oil  Uta Passow and Edward B. Overton	)9
Physiological Responses of Fish to Oil Spills  Martin Grosell and Christina Pasparakis	37
New Microbial Biodiversity in Marine Sediments  Brett J. Baker, Kathryn E. Appler, and Xianzhe Gong	51
Production of Extracellular Reactive Oxygen Species by Marine Biota  Colleen M. Hansel and Julia M. Diaz	77
Variations in Ocean Mixing from Seconds to Years  **James N. Moum**  20	)1
Oceanic Frontogenesis  James C. McWilliams 22	27
Combining Modern and Paleoceanographic Perspectives on Ocean Heat Uptake	
Geoffrey Gebbie	55
Historical Estimates of Surface Marine Temperatures  Flizabeth C Kent and John 7 Kennedy 28	33

Marine Heatwaves  Eric C.J. Oliver, Jessica A. Benthuysen, Sofia Darmaraki, Markus G. Donat,  Alistair J. Hobday, Neil J. Holbrook, Robert W. Schlegel, and Alex Sen Gupta	313
Turbulence and Coral Reefs  Kristen A. Davis, Geno Pawlak, and Stephen G. Monismith	343
The Hydrodynamics of Jellyfish Swimming  John H. Costello, Sean P. Colin, John O. Dabiri, Brad J. Gemmell,  Kelsey N. Lucas, and Kelly R. Sutherland	375
Marine Parasites and Disease in the Era of Global Climate Change  *James E. Byers***	397
Incorporating Biological Traits into Conservation Strategies  Marta Miatta, Amanda E. Bates, and Paul V.R. Snelgrove	421
Emerging Solutions to Return Nature to the Urban Ocean  Laura Airoldi, Michael W. Beck, Louise B. Firth, Ana B. Bugnot,  Peter D. Steinberg, and Katherine A. Dafforn	445
Ocean Optimism: Moving Beyond the Obituaries in Marine Conservation Nancy Knowlton	479
Amazon Sediment Transport and Accumulation Along the Continuum of Mixed Fluvial and Marine Processes  Charles A. Nittrouer, David J. DeMaster, Steven A. Kuehl, Alberto G. Figueiredo Jr., Richard W. Sternberg, L. Ercilio C. Faria, Odete M. Silveira, Mead A. Allison, Gail C. Kineke, Andrea S. Ogston, Pedro W.M. Souza Filho, Nils E. Asp, Daniel J. Nowacki, and Aaron T. Fricke	501
The Origin of Modern Atolls: Challenging Darwin's Deeply Ingrained Theory André W. Droxler and Stéphan 7. Jorry	537

### Errata

An online log of corrections to *Annual Review of Marine Science* articles may be found at http://www.annualreviews.org/errata/marine